

# Flow visualization at extremely low Reynolds number

MIGUEL A. BARCALA-MONTEJANO<sup>1</sup> ([miguel.barcala@upm.es](mailto:miguel.barcala@upm.es)), ÁNGEL A. RODRÍGUEZ-SEVILLANO<sup>1</sup> ([angel.rodriguez.sevillano@upm.es](mailto:angel.rodriguez.sevillano@upm.es)), RAFAEL BARDERA-MORA<sup>2</sup> ([barderar@inta.es](mailto:barderar@inta.es)), RAQUEL ALONSO-CASTILLA<sup>1</sup> ([raquel.alonso.castilla@alumnos.upm.es](mailto:raquel.alonso.castilla@alumnos.upm.es)), LAURA FUENTES-GIL<sup>1</sup> ([laura.fuentes.gil@alumnos.upm.es](mailto:laura.fuentes.gil@alumnos.upm.es)) AND JOSE RIBELLES-FAYOS<sup>1</sup> ([jose.ribelles.fayos@alumnos.upm.es](mailto:jose.ribelles.fayos@alumnos.upm.es))

<sup>1</sup> Escuela Técnica Superior de Ingeniería Aeronáutica y del Espacio  
Universidad Politécnica de Madrid.  
Plaza del Cardenal Cisneros, 28040 MADRID, Spain.

<sup>2</sup> Instituto Nacional de Técnica Aeroespacial (INTA)  
Carretera de Ajalvir, km 4,5. 28850 Torrejón de Ardoz (MADRID), Spain

## Abstract

Visualization techniques have supported theoretical concepts since the beginning of fluid mechanics. Flows at extremely low Reynolds number ( $\sim 10^3$ ) have risen in importance since the release of micro air vehicles and space exploration in other planetary atmospheres, like Mars atmosphere. This paper presents the main results obtained with visualization techniques over bluff bodies and three-dimensional vortex generators. With the measurements obtained, conclusions have been established about stall patterns, evolution of streamlines around 3D bodies and three-dimensional turbulence over a columnar vortex generator (CVG). Visualization techniques will be revealed as complementary but essential tools to understand these phenomena.

## 1. Introduction

Flow visualization is an experimental technique dating from Leonardo Da Vinci age (1452-1519), which has made and keeps making possible the study of complex flows around bodies from diverse scientific and engineering fields. Within the visualization techniques, this project is focused on fluids observation through dye injection, one of the oldest techniques used for the analysis and comprehension of fluid mechanics. Besides, its simplicity and easy implementation allow to make visible the streaklines allowing the observation of phenomena that are not fully understood and that would not have been possible to study with other techniques [1].

Osborne Reynolds was one of the scientifics that, in 1883, used this method to characterize the flow inside a circular pipe, establishing the differences between laminar and turbulent flows and studying the transition among them. Reynolds also defined the non-dimensional parameter that characterizes the movements shown in this paper, the Reynolds number ( $Re$ ), which represents the relation between inertial and viscous forces as a function of the fluid density ( $\rho$ ) and viscosity ( $\mu$ ), the free-stream velocity ( $U_\infty$ ) and a reference length ( $D$ ):

$$Re = \frac{\rho \cdot U_\infty \cdot D}{\mu} \quad (1)$$

In this particular study of visualization in water, low velocities and the small dimensions of the tested models lead extremely low Reynolds values comprised from 193 to 5200. This low  $Re$  regime is more typical of the Mars atmosphere flight and the emerging market of drones than the commercial aeronautical business, so the existing literature in this regard is scarce. A research shows that low Reynolds number flows are highly viscous and some effects increase when Reynolds number decreases [2]. Accordingly, the decision has been made to use this technique in order to characterize the flow structure around a building and a ski-jump of an aircraft carrier and reduce the hazard level to the aircraft that land and take off in these platforms.

Aircraft carriers constitute a key strategic tool for the projection of the aerial power in remote places, with high mobility and flexibility through the open sea. This type of ships serve as transportation for aircraft, both rotary-wing and fixed-wing, enabling their launch and recovery. On occasions, aircraft carriers have ski-jump ramps to allow aircraft reach the needed lift for the flight, either with a shorter take-off run or with lower take-off weight, significantly improving

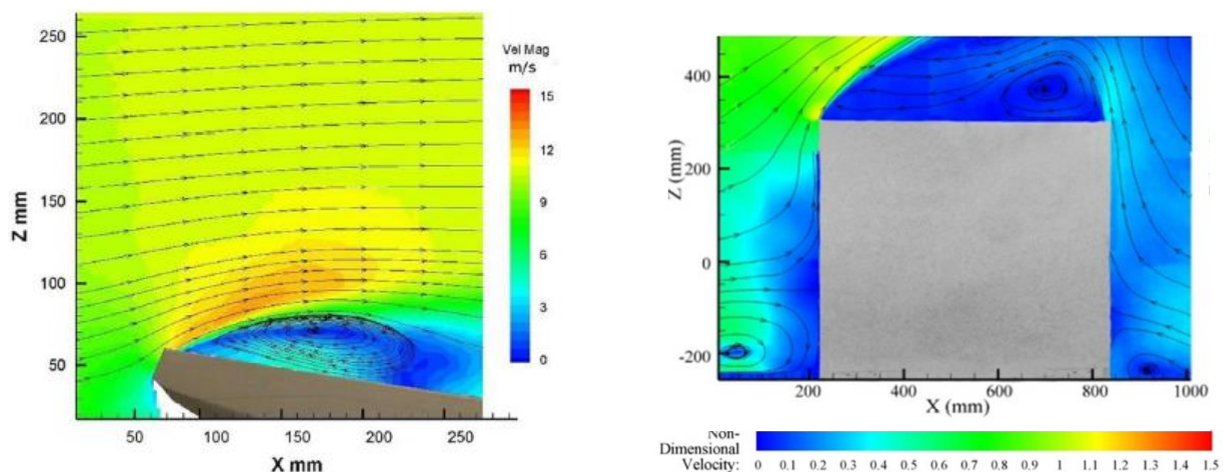
their performance. A study from de US demonstrated that this system was able to reduce the ground roll of a McDonnell Douglas F-18 in more than 50% [3].

For its part, some buildings present heliports on their roofs that, despite their compact dimensions, permit access of helicopters for emergency and security services or private entities. Nevertheless, both buildings and ski-jumps are blunt bodies with their associated aerodynamic phenomenology, which is the source of vortex and unstable flow.

### 1.1 Aerodynamics of buildings and ski-jumps

Considering a wind direction of  $\beta = 0^\circ$ , which means that the wind is perpendicular to the upwind face, the bluff shapes of buildings and ski-jumps lead the immediate detachment of the boundary layer when surpassing the sharp edges, leaving a turbulent wake downstream. The separated flow can also reattach to the surface resulting in a recirculation bubble in the lower part, with flow acceleration in the upper part, which generates intense suction forces [4] [5]. This is illustrated in the following *Figure 1*.

Flying into turbulence may set off a sudden lift variation, giving rise to a loss of control of the aircraft similar to a gust effect. This is in addition to the risk derived not only from the proximity of the aircraft to the building/ship, but also from the still low altitude reached [6]. In the particular case of aircraft carriers, the presence of a strong airflow with a vertical component at the moment of leaving the ski-jump ramp, caused by the high angle of attack, also plays an important and hazardous role. A change in the flow direction over the aircraft may result, at such low speeds, in stall [7].



**Figure 1.** Velocity (m/s) map around a ski-jump without CVG (left) [8]. Non-dimensional velocity map around a building without CVG (right) [4].

This phenomenon has been tried to be minimized through the installation of Columnar Vortex Generators (CVG's). It is a passive flow control device which consists of a spiral shaped open cylinder, closed at one end, with tangential flow ingress and axial flow egress [9]. Its geometry, in *Figure 2*, was designed with the aim of improving the flow quality and mitigate the recirculation bubble that appears when the flow is driven to a sharp edge. Due to this fact, the detachment angle and the height reached by the bubble over the deck/roof will be the parameters under analysis in the present research, comparing three angles of attack for the CVG of the building model ( $\alpha = 0^\circ, 30^\circ, 45^\circ$ ) and two sizes for the CVG of the ski-jump.

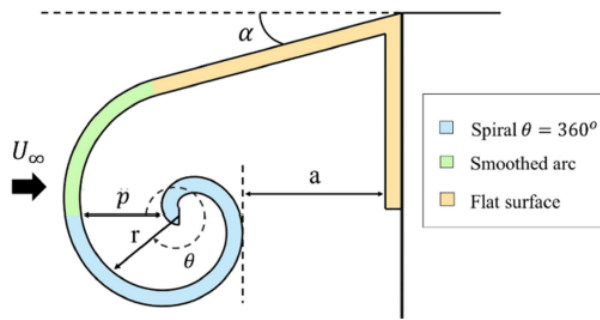


Figure 2. Geometrical parameters of the CVG device [4].

Where:

- $r$ : end radius of curvature
- $\theta$ : angle of the turned
- $p$ : spiral parameter/ pitch
- $\alpha$ : angle of attack
- $a$ : distance to the wall

Geometry defined by:

$$r = \frac{p}{2\pi} \theta$$

The knowledge of the characteristic size of the phenomena occurred is the key for the identification of safe areas for the aircraft operation, so this will be the ultimate goal of the tests. Likewise, this study also tries to illustrate the internal behaviour of the CVG's by performing isolated tests of the device, as well as to diffuse the flow visualization technique in water with dye injection for the analysis of complex flows. Not to mention the need to reveal the growing importance, in the aerospace market, of movements at extremely low Re.

## 2. Experimental details

### 2.1 Test facility and setup

The present task has been developed in the Aerodynamic Laboratory of the School of Aeronautics and Space Engineering (ETSIAE), especially in a towing tank designed and validated by students from this School. The study has been carried out in this tank, through dye visualisation, of different prototypes made by additive manufacturing using 3D printers and which results could be analysed thanks to a varied high-resolution photo acquisition equipment. In all these tests, water is used as the stable fluid where the motion of the models takes place.

The towing tank used for these tests is made up of a main structure of 3000 mm x 410 mm x 410 mm, located at 1500 mm above the floor for a more comfortable visualization and photographing. Additionally, it has an auxiliary equipment needed to carry out the tests. These are depicted in Figure 3.

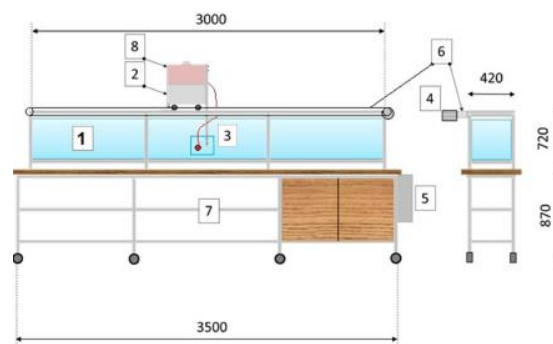


Figure 3. Towing tank overall view. 1. towing tank, 2. model car, 3. model, 4. AC engine, 5. electrical housing, 6. driving belt, 7. towing car structural support, 8. dye tank [1].

The main structure of the towing tank is built with anodised aluminium profiles, which form the structure. They also serve as support for other components such as the rails where the model car displaces. Methacrylate panels join together the aluminium profiles and close the structure allowing to view through.

The model car was designed to transmit the movement from the driving belt to the model and to transport test devices like the dye tank and auxiliary cameras among others. The cited movement takes place thanks to an AC engine, controlled by means of an electrical panel and allowing models motion both forwards and backwards. The velocity of the model and the frequency of the AC engine follow the next linear relationship:

$$U_{\infty} [m/min] = 0.022f_m [Hz] + 0.0565 \quad (2)$$

Where the frequency ( $f_m$ ) range is 0-155 Hz.

This methodology is used for stationary and incompressible flows. In this particular case, streamlines and streaklines overlap and all particles that passes through a certain point follow the same path, so the local velocity vector of each particle is tangent to that line. Therefore, in order to guarantee this condition and get valid test results, it is essential to take the following aspects into consideration:

- 1) Avoid models vibration due to external factors.
- 2) Make sure models have steady motion at constant speed.
- 3) Define a time delay to assure the water is calm.
- 4) Take photographs at the rear of the towing tank, where external disturbances caused when opening the shut-off valve are already cushioned.

## 2.2 Types of dye tracers

Choosing the type of dye is also a relevant factor in tests performance and there are two features to consider: its density and visibility in water.

With the purpose of identifying the flow patterns as clearly as possible, the dye tracer must show a high contrast with the water. The lack of visibility of the dye would induce that the streamlines lose their definition and rapidly disappear, especially in turbulent flows.

Regarding the dye density, it has to be the same or very close to the water density, so the magnitude of the forces acting on the fluid and the dye tracer are identical, guaranteeing the flow is homogeneous. However, density differences can be addressed by adding salt when a density increase is demanded or by adding methanol/ethanol when a density decrease is necessary. Besides, water and dye should be at the same temperature in order to prevent density changes.

Finally, permanganate potassic was chosen as dye tracer for the tests since all requirements are fulfilled. It is a chemical compound in the form of small purple crystals which major advantage is its high solubility in water, so a little amount of substance is needed to do the solution. In addition, permanganate potassic solution is easy to clean and eliminate.

If the dye injection is not carried out in the appropriate conditions, no tracer will follow the correct flow pattern. To prevent this from happening, the following aspects need to be kept in mind [1]:

- 1) The dye injection velocity must not have any perpendicular component to the model's surface.
- 2) The injection has to be made in a laminar regime.
- 3) The model's speed has to be carefully chosen so the dye tracer outlet forms a straight and stable line.

## 2.3 Dye supply

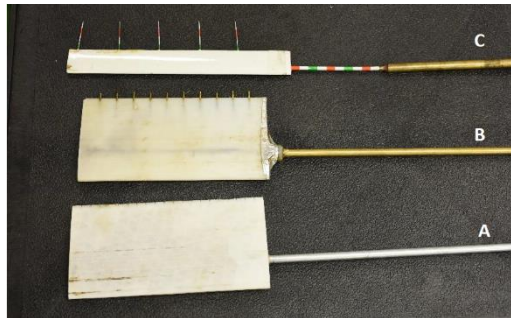
The dye supply system begins at the top of the model car, where a 5 litres recipient is located containing the dye tracer solution. This deposit has a stopcock which opens or closes the flow of the fluid, allowing to be removed for its cleaning and dye preparation. The outlet of the tap connects, through a flexible pipe, to a needle valve that permits to adjust the flow volume according to the speed of the model. This valve leads into the injector pipes which can be part of the model, this is the case of the ski-jump, or be grouped together in an injection rake (I.R.) with an aerodynamic profile shape, like the ones used for the building and CVG models.

The I.R. is located upstream of the model, so its aerodynamic geometry does not perturbate the incident flow. This is a flexible technique that enables to regulate the position, separation, diameter and number of injector tubes just by changing one I.R. for other depending on the test requirements. For the building and CVG tests, the following I.R.'s are detailed in *Table 1*:

**Table 1.** Types of I.R.'s (letters refer to Figure 4).

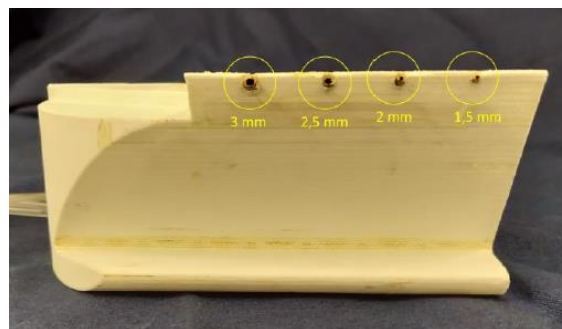
	Nº of tubes	Tubes internal diameter [mm]	Tubes separation [mm]
I.R. A	20	0.4	9
I.R. B	10	0.8	18
I.R. C	5	0.6	42

Figure 4 shows the injection rakes used during the experiments.



**Figure 4.** Injection rakes (I.R.).

This injection method is not valid for frequencies over 15 Hz due to the turbulence increase generated in the dye filaments. Therefore, the ski-jump model has been made with four injectors, each one in a different section of the ramp. From the port to the starboard the diameters are: 1.5 mm, 2 mm, 2.5 mm and 3 mm as it is pictured in Figure 5. After several proofs, the 3 mm injector was determined to be the most appropriate for the tests. Its greater flow volume leads to a major dye flow providing a better visualization, while the injection pressure keeps minimized in order to avoid modifications of the incident stream.



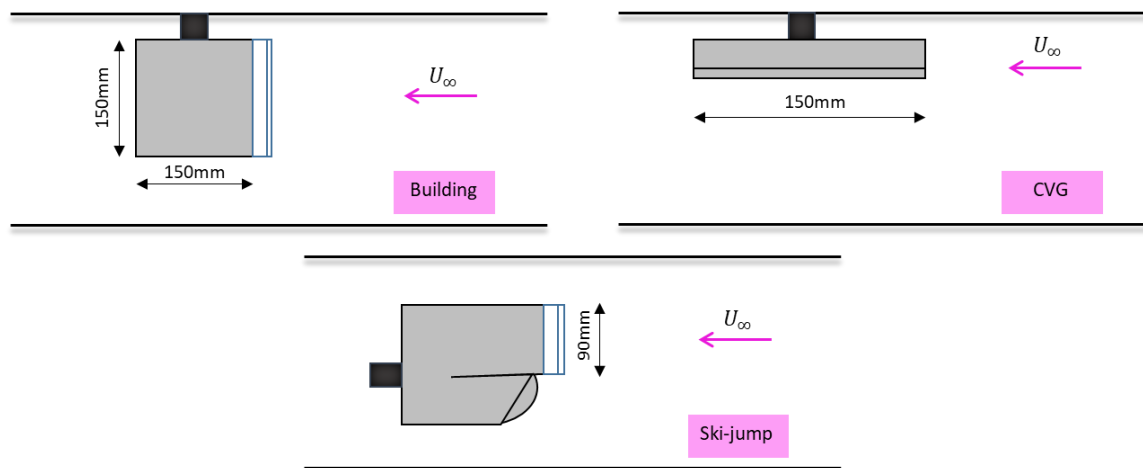
**Figure 5.** Diameters and layout of the ski-jump injectors.

## 2.4 Models positioning

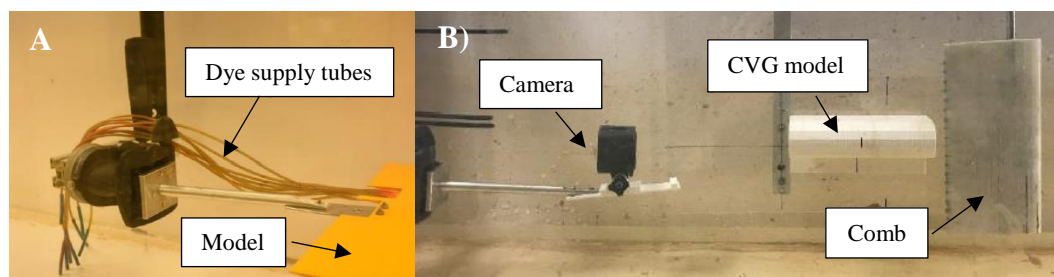
There are two ways of holding the prototypes in the channel, both are shown in Figure 7. One was designed for models which have their own dye injectors, such as the ski-jump. This system has a photograph tripod head joint to an aluminium profile. The tripod head is in turn, united to the model car through a monopod, providing the model's spin in three axes and the simultaneous movement with the prototype along the channel. On occasions, the current mechanism served to support a waterproof camera.

The second model holding system was used for the building and CVG, so the distance to the injector I.R. is minimized and consequently test results are highly precise. It consists of an aluminium square-section tube fixed to one of the model car's profiles through a threaded joint, allowing the rotation of the model. Likewise, prototypes unit to the tube with a screw attachment, ensuring a precise and repetitive position.

Note that in all tests analysed in this paper the incident flow is perpendicular to the upwind face of the model, this is  $\beta = 0^\circ$  (see Figure 6). Therefore, the theoretical background previously exposed always applies.



**Figure 6.** Models positioning in the towing tank.



**Figure 7.** Models holding in the towing tank. A) Ski-jump holding system, B) CVG and building holding system.

### 3. Tested models

#### 3.1 Ski-jump model

A 1:212 scale model of a section of the bow of the ‘Juan Carlos I’ (L-61) aircraft carrier of the Spanish Navy has been used for performing the towing tank test experiments, including the full ski-jump ramp configuration. The ramp of the prototype is 90 mm width, identified from now on with the letter ‘b’, and has a 12° angle of attack.

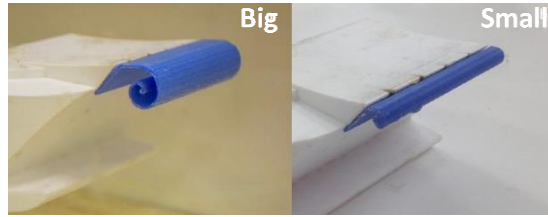


**Figure 8.** Ski-jump model.

The CVG’s installed in the ski-jump were designed following the principle guidelines from previous researches, shown in *Figure 2* and with a length equal to the ski-jump width. However, appropriate changes were made to adapt the original design to the leading edge of the ski-jump. In the first place, the angle of attack ( $\alpha$ ) was modified leading to a tangential extension of the ramp with the device. To do so, a new angle  $\alpha = -45^\circ$  had to be defined. Secondly, the distance to the wall ( $a$ ), arbitrary in the initial design, obeys the expression  $p = a$  and the device dimensions follow the ratio  $p/b$  [8]. Hence, following the literature, two CVG dimensions have been tested as detailed in *Figure 9*.

$$\frac{p}{b} = \frac{1}{30} \rightarrow p = 3 \text{ mm} \rightarrow \text{Small}$$

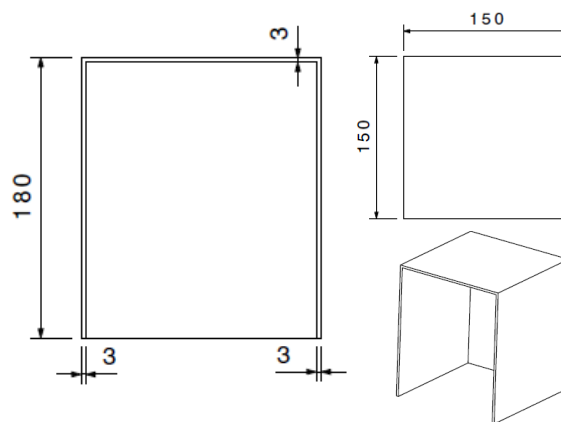
$$\frac{p}{b} = \frac{1}{10} \rightarrow p = 9 \text{ mm} \rightarrow \text{Big}$$



**Figure 9.** CVG's installed in the ski-jump.

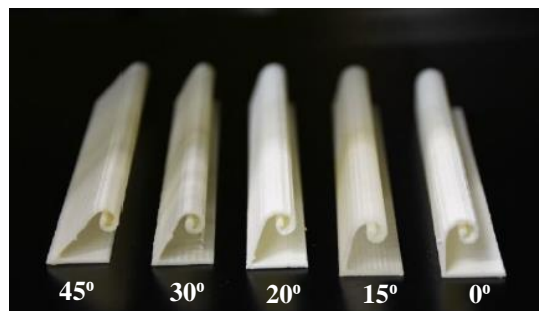
### 3.2 Building model

The building prototype is a prismatic structure composed of three walls and a roof. Everything has been manufactured in a unique piece of dimensions 150 mm x 150 mm x 180 mm (L x W x H) and with a uniform material thickness of 3 mm. The material density was decided to be maximum in order make the structure stiffer and avoid deformations.



**Figure 10.** Building dimensions in mm.

According to the results of the researches done in wind tunnel [4] and considering that the CVG length is the building width ( $W = 150$  mm), the most effective CVG's fulfil the relation  $a/W = 1/20$ . Therefore, three different CVG configurations with three angles of attack ( $\alpha = 15^\circ, 30^\circ, 45^\circ$ ) have been analysed and installed in the building for its comparison, but  $a = 7.5$  mm and  $p = 2.95$  mm have been kept the same in each of them.

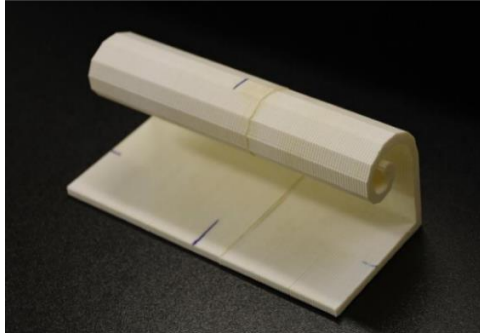


**Figure 11.** CVG's used in the building and their angle of attack.

Both prototypes design, building and ski-jump, represent real sharp-edge structures which lead to flow detachment and the appearance of large recirculation bubbles. The configurations were carefully chosen with the aim of analysing the adverse effects that the aircraft have to deal with in the proximity of these surfaces. Additionally, the present study tries to reveal if the changes occurred with the use of CVG's mitigate the unstable flow conditions typical of these areas.

### 3.3 CVG model

A 4:1 CVG scale model was manufactured from the one attached in the building to carry out isolated tests of the device. As the goal of these tests was getting further information of the CVG internal operation, the analysis was focused in the spiral and the gap dimensions but not in its angle of attack, so  $\alpha = 0^\circ$  was chosen due to its simplicity and its length was kept the same with a value of 150 mm.



**Figure 12.** CVG model device (Scale 4:1).

## 4. Experimental results

In the wake of bluff bodies such as the ski-jump and the building, the presence of Kelvin-Helmholtz instabilities (KHI) indicates the existence of a shear layer which separate fluid regions with different velocities. Therefore, the KHI dyed in the tests delimitate the bubble shape enabling taking quantitative measurements. In particular, two different parameters were selected to characterize the aerodynamic flow and compare the effects of the various CVG devices: the bubble height and the detachment angle of the flow. Measurement criteria are detailed in the corresponding model results sections numbered as 4.1 and 4.2.

### 4.1 Ski-jump results

With the purpose of comprehending and looking for the optimal solution to the high vorticity and flow detachment in ski-jump ramps, three different configurations have been analysed: reference case (i.e.: no CVG's installed), ski-jump with the small CVG (CVG-S) and with the big CVG (CVG-B). Each of them has been tested for three Reynolds numbers: 844, 2725 and 5200.

To get these data Eq (1) has been applied, where the water properties are  $\rho = 1000 \text{ kg/m}^3$ ,  $\mu = 10^{-3} \text{ N}\cdot\text{s/m}^2$  and the ramp width,  $b = 90 \text{ mm}$ , has been taken as the characteristic length. The model velocities  $U_\infty$  have been set to low values to get good image properties and to a higher rate closer to the reality. This is shown in *Table 2*.

**Table 2.** Ski-jump testing conditions.

Frequency [Hz]	$U_\infty$ [m/min]	Re
23	0.56	844
80	1.82	2725
155	3.47	5200

The tests were conducted with no sideslip angle so the incoming flow is perpendicular to the CVG length. The testing results are shown in *Table 3*.

Attending to the qualitative analysis of the photographs in *Table 3*, the most interesting details of the experiments are related to the morphology of the turbulence generated behind the ramp in the absence of passive flow control devices. When the Reynolds of the test is lower than the critical Reynolds ( $Re < 1300$ ), the vortices belonging to the shear layer rolled up to form the detached vortices from the Von Karman street with a larger characteristic size and further downwash.



However, for greater Reynolds ( $Re > 1300$ ) the instabilities develop independently to the Von Karman vortices street. When Reynolds number increases, the flow becomes turbulent and the shear layer is more susceptible to destabilize, so small vortices begin to be generated closer to the detachment point. These are clearly differentiated from the greater ones from the Von Karman street.

**Table 3.** Ski-jump testing results with dye visualisation.










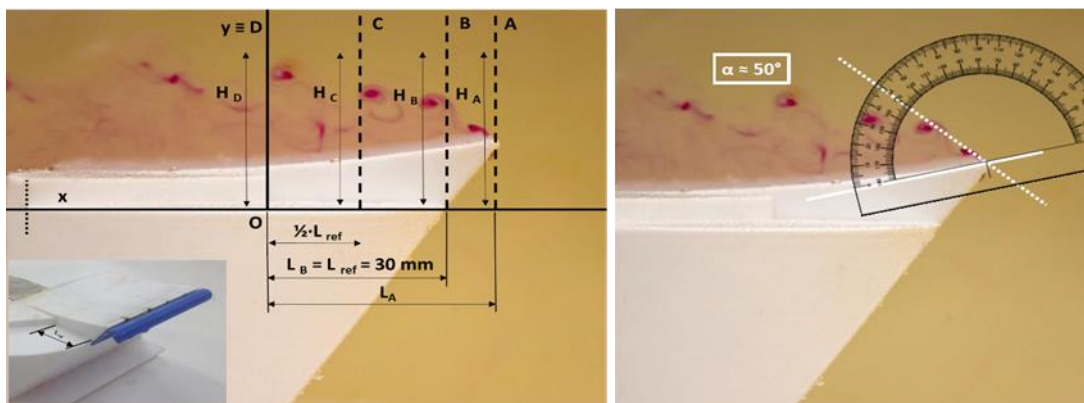
	Re = 5200	Re = 2725	Re = 844
CVG-B			
CVG-S			
Reference Case			

Figure 14 and Table 4 compare all test cases under study at each Re, where the detachment angle of the stream and the height of the recirculation bubble have been measured. To do so, firstly a reference plane where measurements are projected in true size has been defined. This is the right-side surface of the ramp due to its parallelism with the photograph plane. Secondly, it has been established a reference distance ( $L_{ref} = 30$  mm) contained in the cited surface as the region where measurements are taken.



**Figure 13.** Measurement criteria for the bubble height (left) and the detachment angle of the flow (right).

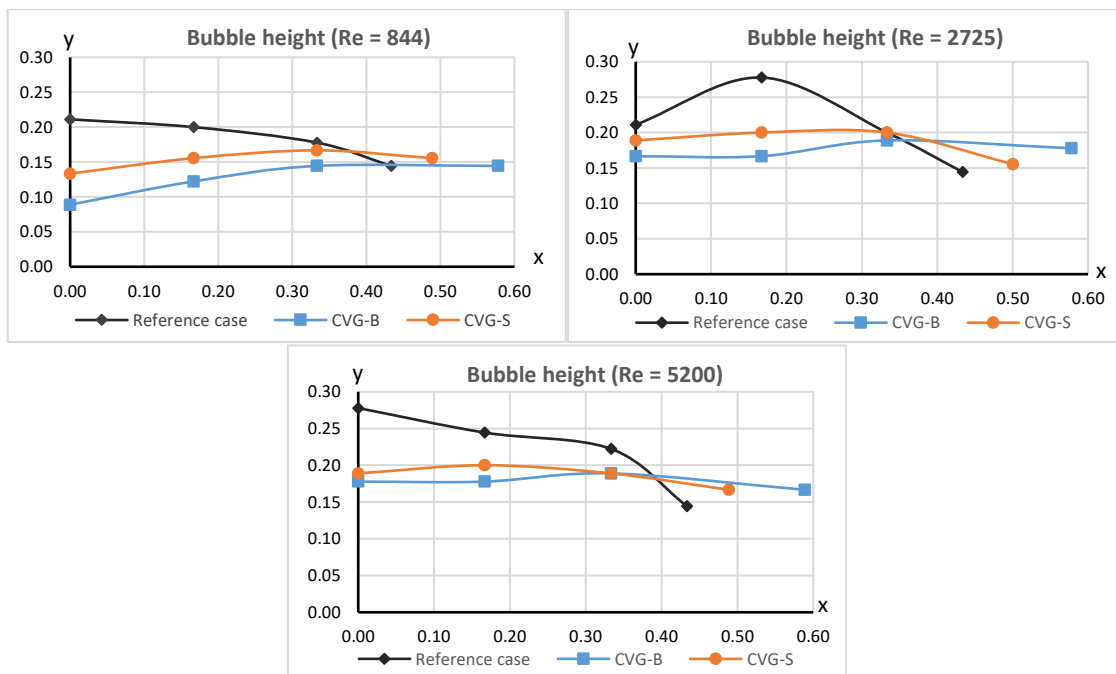
According to the description in Figure 13 (left), the axis used to measure the bubble height are linked to the aircraft carrier and have the origin (O) in the lower-left corner of the reference surface. The abscissa axis is always parallel to the incident stream and has the opposite direction.

The measuring points of the bubble height in the different verticals of the scheme (A-D) are either the height of the closest instability centre of the shear layer or the height of the most external dyed streamline. Meanwhile, the x-coordinate of the vertical in A ( $H_A$ ) is variable and always corresponds to the origin of the detachment, which could be in the ski-jump or in the CVG device. Note that all distances are presented as non-dimensional results where the ramp width has been used as the reference length.

On the other hand, in order to measure the detachment angle, one just has to draw a tangent line to the outer contour of the bubble from the last position where the flow is attached to the surface of the ship or device, like it is shown in Figure 13 (right).

**Table 4.** Detachment angle in the ski-jump model.

	Re = 844	Re = 2725	Re = 5200
CVG-B	0°	5°	5°
CVG-S	0°	20°	10°
Reference case	15°	30°	30°



**Figure 14.** Evolution of the bubble height in the ski-jump at 844, 2725 and 5200 Reynolds number.

The pictures reveal that the use of CVG's leads to a remarkable reduction not only of the bubble size but also of the detachment angle. The effectiveness of the device seems to improve with its size and with the decrease of the speed, which is directly related to the Re. Going over the existing literature, it has been proved that the radius of the curvature of the CVG has a direct effect on the flow detachment in the flight deck [10]. Supporting this idea, the present test results demonstrate that the big CVG actually reduces the detachment angle in 83% with respect to the reference case for a 2725 and 5200 Reynolds number and completely eliminates it when Re = 844.

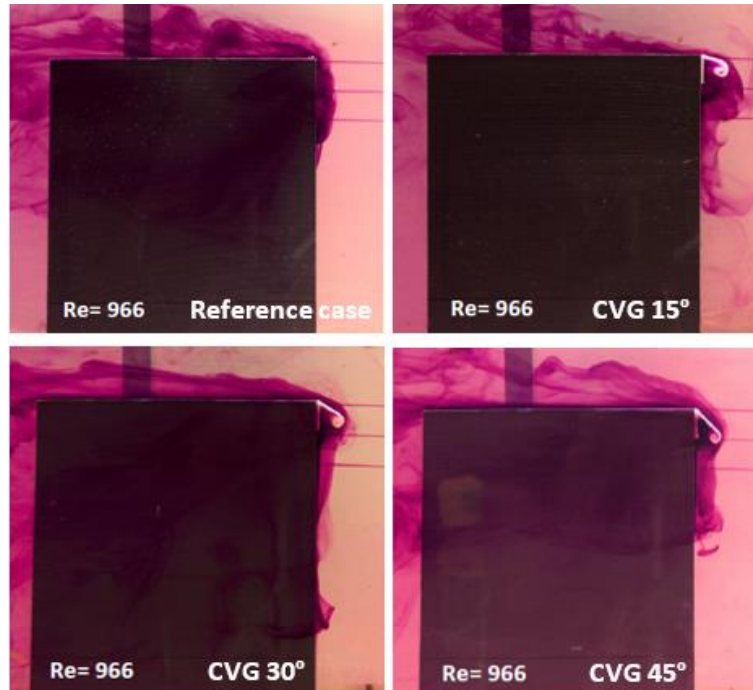
## 4.2 Building results

In this study, the reference case and all the CVG configurations ( $\alpha = 15^\circ, 30^\circ, 45^\circ$ ) have been tested for the same incidence angle of wind  $\beta = 0^\circ$ . This means that the flow is always perpendicular to the upwind wall of the building and the fluid enters tangentially in the device. The flow volume and velocity keep constant and considering the roof width as the characteristic length of the model ( $W = 150$  mm), the Reynolds number of the tests is 944, which asserts that its value is lower than the critical Reynolds for bluff bodies. This extremely low Re was the optimal for a laminar and stable dye injection with the I.R.

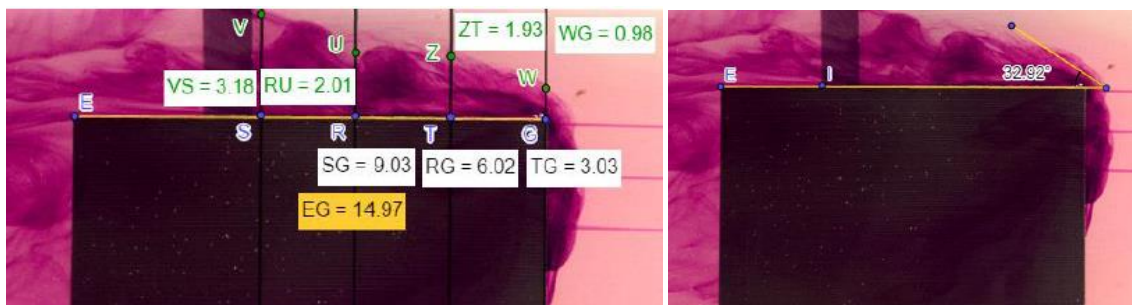
**Table 5.** Building testing conditions.

Frequency [Hz]	$U_\infty$ [m/min]	Re
15	0.39	944

The experimental results obtained during the towing tank tests are represented in *Figure 15*. Attending to the reference case, the streamlines show a great detachment area caused by the sharp edge of the building. Meanwhile, a high-vorticity recirculation bubble is generated over the roof. It is clear that, overall, flow detachment and turbulence are widely mitigated with the installation of the passive flow control devices, but a parametrical analysis is required for a precise comparison and definition of the CVG's behaviour.

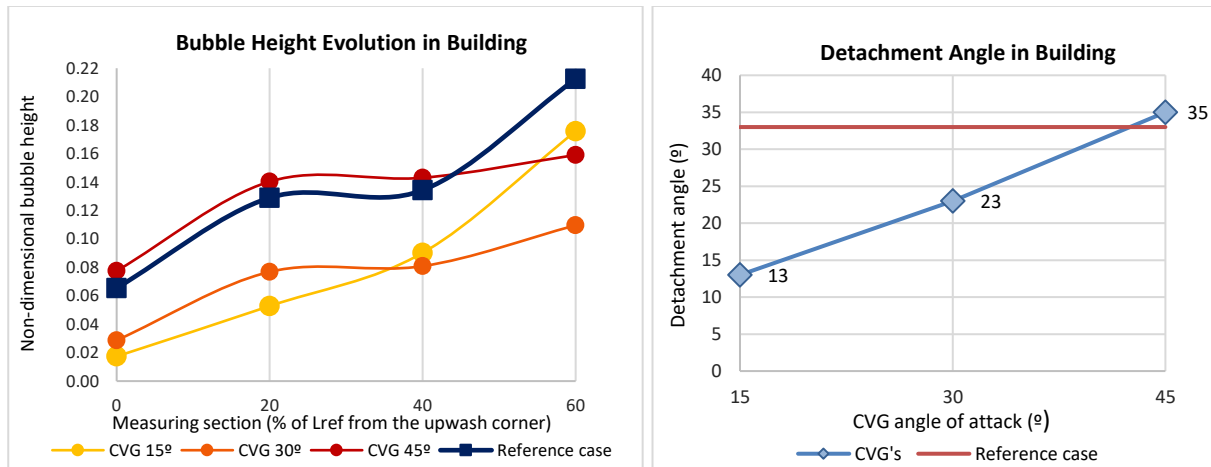
**Figure 15.** Building testing results with dye visualization.

Following the same scheme as the ski-jump, the angle of deflection of the flow and the bubble height have been measured from the figure above, which results are plotted in *Figure 17*. To do so, the right-side wall of the building has been considered as the reference surface where measures are in true size and its upper edge as the reference length ( $L_{ref} = EG = 150$  mm) from where the bubble heights are measured.

**Figure 16.** Measurement criteria for the bubble height (left) and the detachment angle of the flow (right).

In order to quantify the height reached by the flow with respect to the roof for each configuration, it has been established the procedure in *Figure 16* (left). With the origin in the corner G, four heights have been measured at 0%, 20%, 40% and 60% of the total building width ( $W = EG = 150$  mm), corresponding to the segments from WG to VS, respectively.

These segments are perpendicular to the reference line in yellow and ends at the outer contour of the shear layer. Notice that even though the distances represented in *Figure 16* are in cm, the ones in *Figure 17* are non-dimensional obtained dividing by the building width. Meanwhile, the detachment angle is obtained as *Figure 16 (right)* depicts.

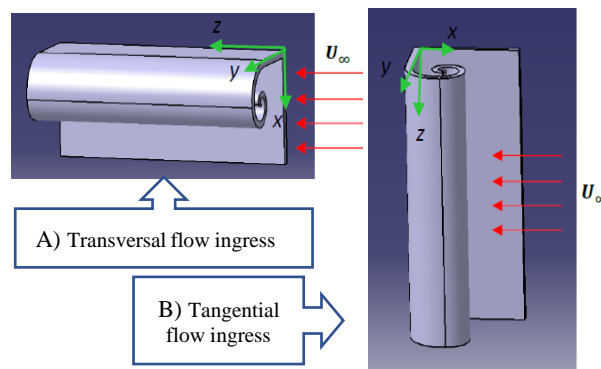


**Figure 17.** Evolution of the bubble height (left) and the detachment angle (right) in the building for  $Re = 944$ .

By focusing on *Figure 17 (right)*, it can be extracted that the detachment angle at the corner of the reference case is  $33^\circ$  and encouraging results are obtained with the use of  $15^\circ$  and  $30^\circ$  CVG's, which provide 62% and 33% of decrease of this angle, respectively. Nevertheless, the  $45^\circ$  CVG aggravates the initial design of the building with a  $35^\circ$  of stream deflection. So, apparently, the lower the CVG inclination ( $\alpha$ ) is, the easier for the flow is to adapt to the new geometry. When expanding the view to other sections of the roof, one can discern the sudden and sharp rise of the flow, both in the reference case and with the  $15^\circ$  CVG, especially when it reaches the 40% section. Meanwhile, the  $30^\circ$  and  $45^\circ$  devices show a stable behaviour of the bubble region. In spite of this fact, as *Figure 17 (left)* shows, the  $45^\circ$  CVG leaves a great detachment above the roof, even more pronounced than the reference case overall. Hence, the  $30^\circ$  CVG is the most effective one of those studied due to the high attachment of the flow it presents and the laminar condition of that flow that can be observed in *Figure 15*.

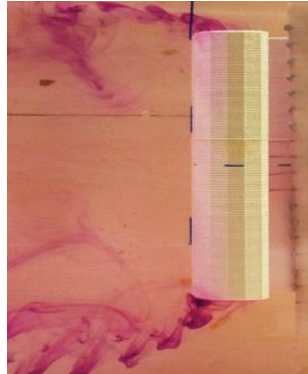
### 4.3 CVG results

Two types of tests were developed to prove the CVG concept. Ones with tangential flow ingress (*Figure 18b*), where the goal was to ascertain if the axial flow captured through the gap would interact with the spiral construction leading to a vortex at the open end [9]. Others with transversal flow ingress through the spiral (*Figure 18a*) in order to visualize the flow direction of rotation. The results of this research would provide a deep knowledge of the CVG operation by analysing the fluid trajectory within the device. Thus, its geometry could be optimized for a more efficient use in different applications.



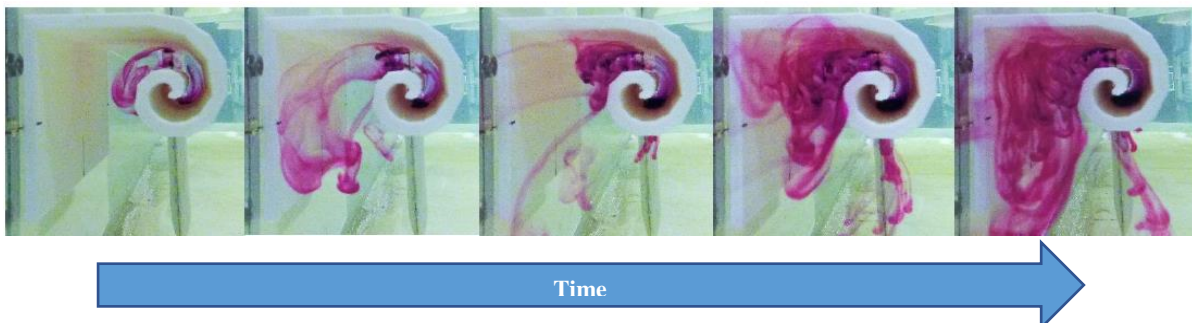
**Figure 18.** Types of tests developed with the isolated CVG.

In this study, the frequency of the towing tank engine was fixed at 15 Hz, exactly the same as in the building research due to the dye supply technique used. Meanwhile, the distance to the wall ( $a = 30$  mm) was selected as the characteristic length of the device, so the Reynolds of the tests is 193.



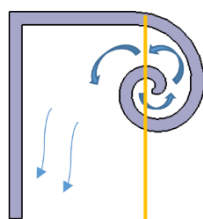
**Figure 19.** CVG testing result with dye visualization and tangential flow ingress.

As *Figure 19* demonstrates, when a tangential flow ingress takes place the flow egress in analogous in both extremes of the device, not only in quantity but in form as well. Small wake vortices appear possibly due to the fact that the fluid penetrates inside the CVG spiral with a turning tendency that accompanies its geometry. These vortices, with a remaining rotational component in their velocity, persist downstream. In this way, the flow is redirected to the open bases of the cylinder instead of through the gap to the exterior longitudinal surface, where the deck of a ship or the roof of a building would be located. Consequently, the more fluid is drained by the CVG, the weaker the stream is in the proximity of these platforms and the less hazardous is for the aircraft to manoeuvre in that area.



**Figure 20.** Flow rotation inside the CVG.

*Figure 20* sets out a chronological image sequence captured from the tests and which shows the pathlines inside the CVG. The dark purple areas indicate the accumulation of the dye and therefore, the most repetitive trajectory of the fluid. Hence, according to the photographs one can appreciate how the flow begins to gather in the centre of the spiral and then, spreads to the left-vertical wall. Considering that the images have been taken from the back (downwash of the model), it is a turn of the fluid in  $Z^+$ .



**Figure 21.** Flow direction of rotation inside the CVG.

## 4. Conclusions

Rotary and fixed wing aircraft often have to deal with a high turbulence and vorticity near of some landing and take-off platforms, such as buildings heliports and ski-jump rumps in aircraft carriers. The unstable flow related to the bluff-body condition forces pilots to face real challenges when manoeuvring in their proximities, which has triggered the present research. This paper studies the flow field over a 150x150x180 mm building and a 1:212 scale model of the 'Juan Carlos I' aircraft carrier bow in the presence of a ski-jump. Different passive actuators have been tested with the aim of directing and organizing the flow so the recirculation bubble that appears on the roof and ramp is mitigated. The particular small dimensions of the models and the low speeds of the tests lead to extremely low Reynolds number movements ( $10^2$ - $10^3$ ), which result in the magnification of the aerodynamic phenomena occurred and the facilitation of the analysis. A visualization technique through dye injection in water together with a high-quality photo equipment have been used to determine the detachment angle of the flow and the evolution of the bubble height along the corresponding surface.

The results obtained for the ski-jump reveal that the CVG-B ( $p/b = 1/10$ ) shows the best performance with an 83%-100% decrease of the detachment angle and a great mitigation of the bubble that leaves a laminar flow downwash. The effectiveness of this device not only improves with the size but also with the reduction of the Re. On the other hand, the building sharp edges generate a stream deflection of  $33^\circ$  on the roof, so the need of CVG's is essential. While the  $15^\circ$  CVG shows the biggest reduction of the detachment angle in the corner, the  $30^\circ$  CVG seems to achieve the greatest improvement in the evolution of the flow on the roof at the time that reduces the initial deflection in 33%. The high vorticity that leads to an increase of the bubble size when using the  $15^\circ$  CVG, compared to the stable and uniform flow after the  $30^\circ$  CVG makes it the most effective one. Finally, it was proved that the incoming flow interacts with the spiral of the CVG following a  $Z^+$  rotation and driving the fluid to the laterals where it abandons the device with small remaining vortices. This trajectory would divert most of the flow out of the area of interest destined for the aircraft flight.

It is clear that the methodology used is able to reveal complex flow behaviours that computational tools may not be able to predict in such an accurate way. Future investigations could demonstrate the reliability of this technique at low Re by developing micro air vehicles (MAV) tests which would provide encouraging contributions to this emerging and powerful market.

## References

- [1] Rodríguez-Sevillano, Á. A., Barcala Montejano, M. A., Bardera Mora, R., & Batuecas Fuejo, J. (2017). Flow Study over Bluff Bodies Based on Visualization Technique. *American Journal of Science and Technology*, 4(6), 97-104.
- [2] Sun, Q., & Boyd, I. (2004). Flat-plate aerodynamics at very low Reynolds number. *Journal of Fluid Mechanics*, 502, 199-206. doi:10.1017/S0022112003007717.
- [3] Turner, E. W. (1991). Aircraft Operations from Runways with Inclined Ramps (Ski-Jump) (No. WRDC-TM-90-337-FIBE). Wright Research and Development Center Wright-Patterson AFB OH.
- [4] Bardera Mora, R., Barcala Montejano, M. A., Rodríguez-Sevillano, Á. A., León Calero, M., & Matías García, J. C. (2018). Passive Flow Control over the Roof of Buildings by Using Columnar Vortex Generator. *International Journal of Civil Engineering and Construction Science*, 5(1), 32-42.
- [5] Frank, M. W. *Mecánica de fluidos*, Sexta Edición 2008 McGraw-Hill Interamericana de España. SAU [Consulta: 17/12/2015].
- [6] Fresh, I. N. (1945). Airflow tests over flight deck of 1/48-scale model of CVL 48 with various leading edges. Washington, D.C.: Navy Department.
- [7] Yangang, W., Weijun, W., & Xiangju, Q. (2013). Multi-body dynamic system simulation of carrier-based aircraft ski-jump takeoff. *Chinese Journal of Aeronautics*, 26(1), 104-111.
- [8] Bardera, R., Rodríguez-Sevillano, A., León-Calero, M., & Nova-Trigueros, J. (2018). Three-dimensional characterization of passive flow control devices over an aircraft carrier ski-jump ramp. *Proceedings of the Institution of Mechanical Engineers, Part G: Journal of Aerospace Engineering*, 232(15), 2737-2744.

- [9] Landman, D., Lamar, J. E., & Swift, R. (2005). Particle image velocimetry measurements to evaluate the effectiveness of deck-edge columnar vortex generators on aircraft carriers.
- [10] Kelly, M. F., White, M. D., Owen, I., & Hodge, S. (2016). The Queen Elizabeth Class Aircraft Carriers: Airwake Modelling and Validation for ASTOVL Flight Simulation.